Available online at www.sciencedirect.com
SCIENCE DIRECT®
International Journal of Solids and Structures 42 (2005) 1705–1727
INTERNATIONAL JOURNAL OF SOLIDS and STRUCTURES
www.elsevier.com/locate/ijsolstr

Unconventional friction theory based on the subloading surface concept

K. Hashiguchi *, S. Ozaki, T. Okayasu

Graduate School of Bio-production and Environmental Sciences, Kyushu University, Hakozaki 6-10-1, Higashi-ku, Fukuoka 812-8581, Japan

Received 12 January 2004; received in revised form 6 August 2004
Available online 7 October 2004

Abstract

A constitutive model for the description of friction phenomena is formulated by incorporating the concept of the *subloading surface* [Hashiguchi, K., 1978. Plastic constitutive equations of granular materials. In: Proc. US–Japan Seminar Continuum Mech. Stast. Appr. Mech. Granular Materials, Sendai, pp. 321–329; Hashiguchi, K., 1980. Constitutive equations of elastoplastic materials with elastic–plastic transition. J. Appl. Mech. (ASME) 47 (1980) 266–272; Hashiguchi, K., 1989. Subloading surface model in unconventional plasticity. Int. J. Solids Struct. 25 (1989) 917–945] falling within the framework of *unconventional plasticity* [Drucker, D.C., 1988. Conventional and unconventional plastic response and representation. Appl. Mech. Rev. (ASME) 41 (1988) 151–167], which excludes the premise that the interior of a yield surface is a purely elastic domain. It describes the nonlinear relationship between the normal and tangential tractions on a contact surface. Furthermore, it predicts the gradual progress of sliding displacement with an increase in traction, and thus a judgment regarding the fulfillment of the sliding condition is not necessary. This is in contrast to a conventional friction model with a sliding surface enclosing an elastic domain, in which such gradual progress cannot be described and the judgment is required. Thus, a rough numerical calculation with large loading steps even in the explicit numerical method is allowed in the present friction model. In addition, typical friction boundary value problems are analyzed by the finite element method incorporating the present friction model.

Keywords: Constitutive laws; Plasticity; Friction; Subloading surface model; Finite element method

* Corresponding author. Tel.: +81 92 642 2927; fax: +81 92 642 2932.
E-mail address: khashi@bpes.kyushu-u.ac.jp (K. Hashiguchi).

0020-7683/$ - see front matter © 2004 Elsevier Ltd. All rights reserved.
doi:10.1016/j.ijsolstr.2004.08.006

1. Introduction

In the last quarter century, considerable effort has been invested in describing friction phenomena between solids. In particular, the sliding velocity has been formulated by a rigid perfectly plastic constitutive equation adopting the plastic flow rule by Seguchi et al. (1974), Fredriksson (1976), and Michalowski and Mroz (1978). This has been extended by Curnier (1984), Cheng and Kikuchi (1985), Wriggers et al. (1990), and Peric and Owen (1992) to be described by an elastic perfectly plastic constitutive equation, which incorporates the penalty parameters representing fictitious springs between contact surfaces. Let this be called the *conventional friction model* in accordance with Drucker's (1988) definition of the plasticity with the yield surface enclosing a purely elastic domain. However, many problems remain unsolved. Among them are the following fundamental problems that have to be solved for the development of analyses of engineering ones.

(1) In *Coulomb's friction law*, which has been widely used since early times, the relationship between the normal and the tangential tractions on the contact surface between solids are related linearly. However, this law does not appropriately describe the real frictional traction since in fact the relationship is slightly nonlinear: the increase in the tangential traction gradually weakens with the increase in the normal traction. In other words, Coulomb's friction law cannot appropriately describe the traction on the contact surface over a wide range.
(2) It had been assumed that sliding displacement occurs suddenly when the traction fulfills the *sliding condition* that describes the traction for which sliding occurs in classical models. This assumption was later modified such that sliding displacement first occurs elastically and thereafter the plastic sliding displacement participates suddenly when the sliding condition of conventional models is fulfilled. In fact, however, sliding displacement progresses gradually as the tangential traction increases, exhibiting a smooth relationship between the tangential traction and the relative tangential displacement, i.e., there is a smooth *elastic–plastic transition*. Thus, the description of the frictional coefficient as a monotonically increasing function of relative tangential displacement was adopted by Rabinowicz (1951, 1965), Burwell and Rabinowicz (1953), Johnson (1955), Courtney-Pratt and Eisner (1957), Banerjee (1968), Johannes et al. (1973), Oden and Pires (1983), Cheng and Kikuchi (1985), and many others. However, such a simple method that follows from the formulation of the elastoplastic constitutive equation is applicable only to monotonic frictional loading.
(3) Because of deficiency (2), the accumulation of sliding displacement for cyclic loading of tangential traction inside the surface prescribing the sliding condition, called the *sliding surface*, cannot be predicted.
(4) Also because of deficiency (2), a judgment whether or not a traction fulfills the sliding condition is required.
(5) The inverse relation, i.e., the expression of the relative velocity in terms of the traction rate, cannot be formulated since the rate of contact traction is indeterminate in the plastic sliding process, exhibiting a perfectly plastic state.

In the last several decades, the elastoplastic constitutive equation, falling within the framework of *unconventional plasticity* (Drucker, 1988) that excludes the premise that the interior of a yield surface is a purely elastic domain, has been developed to describe the plastic strain rate due to the rate of stress inside the yield surface by the *subloading surface model* (Hashiguchi, 1978, 1980, 1989). This model introduces the *subloading surface*, which always passes through the current stress and keeps similarity to the yield surface. Then, it is assumed that the plastic strain rate progresses as the ratio of the size of the subloading surface to that of the yield surface increases. This model always fulfills the *smoothness condition* (Hashiguchi, 1993a,b, 1997, 2000) and exhibits a smooth *elastic–plastic transition*. The subloading surface model has been widely applied to metals (e.g., Hashiguchi and Yoshimaru, 1995; Hashiguchi et al., 2001) and soils (e.g., Topolnicki,

1990; Hashiguchi and Chen, 1998; Asaoka et al., 2000; Hashiguchi et al., 2002; Hashiguchi and Tsutsumi, 2003), while the friction phenomena is similar to soil deformation behavior since soils exhibit a frictional property with a pressure dependency.

In this article, we formulate a generalized friction theory, called the *subloading-friction model*, that solves all the aforementioned problems in the classical and the conventional models by incorporating the concept of the subloading surface. Furthermore, finite element programming is implemented that incorporates the present model. Typical friction boundary value problems, specifically the compression of a rectangular block, the indentation of a cylindrical rigid roller into an elastic body, and the cyclic friction problem, are analyzed by the finite element program.

2. General formulation of the constitutive equation for friction

The constitutive equation of friction phenomena is formulated in this section incorporating the concept of the subloading surface (Hashiguchi, 1978, 1980, 1989) into the conventional friction model (e.g., Curnier, 1984; Cheng and Kikuchi, 1985; Wriggers et al., 1990; Peric and Owen, 1992), which is often called the *penalty contact formulation*.

2.1. Decomposition of relative velocity

The relative velocity $\mathbf{r}$ between contact surfaces is additively decomposed into the normal component $\mathbf{r}_{\mathrm{n}}$ and the tangential component $\mathbf{r}_{\mathrm{t}}$ as follows:

$$\mathbf{r} = \mathbf{r}_{\mathrm{n}} + \mathbf{r}_{\mathrm{t}}, \tag{1}$$

which are given as

$$\left.\begin{aligned} \mathbf{r}_{\mathrm{n}} &= (\mathbf{r}\bullet\mathbf{n})\mathbf{n} = (\mathbf{n}\otimes\mathbf{n})\mathbf{r}, \\ \mathbf{r}_{\mathrm{t}} &= \mathbf{r} - \mathbf{r}_{\mathrm{n}} = (\mathbf{I} - \mathbf{n}\otimes\mathbf{n})\mathbf{r}, \end{aligned}\right\} \tag{2}$$

where $\mathbf{n}$ is the unit outward-normal vector at the contact surface, $(\bullet)$ and $\otimes$ denote the scalar and the tensor products, respectively, and $\mathbf{I}$ is the identity tensor. Furthermore, it is assumed that $\mathbf{r}$ is additively decomposed into the elastic part $\mathbf{r}^{\mathrm{e}}$ and the plastic part $\mathbf{r}^{\mathrm{p}}$, (sliding velocity), i.e.,

$$\mathbf{r} = \mathbf{r}^{\mathrm{e}} + \mathbf{r}^{\mathrm{p}}, \tag{3}$$

with

$$\left.\begin{aligned} \mathbf{r}_{\mathrm{n}} &= \mathbf{r}_{\mathrm{n}}^{\mathrm{e}} + \mathbf{r}_{\mathrm{n}}^{\mathrm{p}}, \\ \mathbf{r}_{\mathrm{t}} &= \mathbf{r}_{\mathrm{t}}^{\mathrm{e}} + \mathbf{r}_{\mathrm{t}}^{\mathrm{p}}. \end{aligned}\right\} \tag{4}$$

First, let the elastic parts be given by

$$\left.\begin{aligned} \overset{\circ}{\mathbf{f}}_{\mathrm{n}} &= -\alpha_{\mathrm{n}}\mathbf{r}_{\mathrm{n}}^{\mathrm{e}}, \\ \overset{\circ}{\mathbf{f}}_{\mathrm{t}} &= -\alpha_{\mathrm{t}}\mathbf{r}_{\mathrm{t}}^{\mathrm{e}}, \end{aligned}\right\} \tag{5}$$

where $\mathbf{f}_{\mathrm{n}}$ and $\mathbf{f}_{\mathrm{t}}$ are the normal and the tangential components of the traction vector $\mathbf{f}$ applied to a unit area of contact surface, $(\circ)$ denoting the corotational rate with objectivity:

$$\left.\begin{aligned} \overset{\circ}{\mathbf{f}}_{\mathrm{n}} &= \overset{\bullet}{\mathbf{f}}_{\mathrm{n}} - \boldsymbol{\Omega}\mathbf{f}_{\mathrm{n}}, \\ \overset{\circ}{\mathbf{f}}_{\mathrm{t}} &= \overset{\bullet}{\mathbf{f}}_{\mathrm{t}} - \boldsymbol{\Omega}\mathbf{f}_{\mathrm{t}}, \end{aligned}\right\} \tag{6}$$

where $(\bullet)$ is the material-time derivative and the second-order skew-symmetric tensor $\mathbf{\Omega}$ designates the rigid-body rotation of the contact surface, while $\mathbf{r}$ is not an absolute velocity but is the relative velocity having the objectivity. α_n and α_t are penalty parameters representing fictitious elastic moduli in the normal and the tangential directions to the contact surface. Thus, it follows from Eq. (5) that

$$\overset{\circ}{\mathbf{f}} = \overset{\circ}{\mathbf{f}}_n + \overset{\circ}{\mathbf{f}}_t = \mathbf{C}^e\mathbf{r}^e, \tag{7}$$

where the second-order tensor $\mathbf{C}^e$ is the frictional elastic modulus between contact surfaces and is decomposed into the normal and tangential components, i.e.,

$$\mathbf{C}^e = \mathbf{C}^e_n + \mathbf{C}^e_t, \tag{8}$$

with

$$\left.\begin{aligned} \mathbf{C}^e_n &= -\alpha_n \mathbf{n}\otimes\mathbf{n}, \\ \mathbf{C}^e_t &= -\alpha_t(\mathbf{I}-\mathbf{n}\otimes\mathbf{n}). \end{aligned}\right\} \tag{9}$$

2.2. Normal-sliding and sliding-subloading surfaces

Let us assume the following *sliding surface* with isotropic hardening/softening, which describes the *sliding condition*.

$$f(\|\mathbf{f}_n\|, \|\mathbf{f}_t\|) = F(H), \tag{10}$$

where $\|\ \|$ designates the magnitude. The scalar H is the isotropic hardening/softening variable, which prescribes the expansion/contraction of the sliding surface according to the sliding. In what follows, we assume that the interior of the sliding surface is not a purely elastic domain, but that the sliding velocity (plastic relative velocity) is induced by the rate of traction inside that surface. Therefore, let the surface described by Eq. (10) be called the *normal-sliding surface*.

Next we introduce the *sliding-subloading surface*, which always passes through the current traction $\mathbf{f}$ and keeps a similar shape and similarity in its arrangement to the normal-sliding surface with respect to the zero traction point $\mathbf{f}=\mathbf{0}$. These facts possess the following geometrical properties:

(i) All lines connecting an arbitrary point on or within the sliding-subloading surface and its conjugate point on or within the normal-sliding surface join at a unique point, called the *similarity-center* which is the origin of the traction space in the present model.
(ii) All ratios of length of an arbitrary line-element connecting two points on or inside the sliding-subloading surface to that of an arbitrary conjugate line-element connecting two conjugate points on or inside the normal-sliding surface are identical. The ratio is called the *similarity-ratio*, which coincides with the ratio of the sizes of these surfaces.

Let us call the similarity-ratio of the sliding-subloading surface to the normal-sliding surface the *normal-sliding ratio*, denoted by R, where $R=0$ corresponds to the null traction state ($f=0$) as the most elastic state, $0<R<1$ to the *subsliding state* ($0<f<F$), and $R=1$ to the *normal-sliding state* in which the traction lies on the normal-sliding surface ($f=F$). Therefore, the normal-sliding ratio R plays the role of a 3-dimensional measure of the degree of approach to the normal-sliding state.

The sliding-subloading surface is described by

$$f(\|\mathbf{f}_n\|,\ \|\mathbf{f}_t\|) = RF(H). \tag{11}$$

The material-time derivative of Eq. (11) leads to

$$\frac{\partial f}{\partial \|\mathbf{f}_{\mathrm{n}}\|}\mathbf{n}\bullet\overset{\bullet}{\mathbf{f}}_{\mathrm{n}}+\frac{\partial f}{\partial \|\mathbf{f}_{\mathrm{t}}\|}\mathbf{t}\bullet\overset{\bullet}{\mathbf{f}}_{\mathrm{t}}=\overset{\bullet}{R}F+R\overset{\bullet}{F}, \tag{12}$$

where

$$\mathbf{n}=\frac{\mathbf{f}_{\mathrm{n}}}{\|\mathbf{f}_{\mathrm{n}}\|},\ \ \mathbf{t}=\frac{\mathbf{f}_{\mathrm{t}}}{\|\mathbf{f}_{\mathrm{t}}\|}. \tag{13}$$

Eq. (12) is obviously transformed to

$$\frac{\partial f}{\partial \|\mathbf{f}_{\mathrm{n}}\|}\mathbf{n}\bullet\overset{\circ}{\mathbf{f}}_{\mathrm{n}}+\frac{\partial f}{\partial \|\mathbf{f}_{\mathrm{t}}\|}\mathbf{t}\bullet\overset{\circ}{\mathbf{f}}_{\mathrm{t}}=\overset{\bullet}{R}F+R\overset{\bullet}{F}. \tag{14}$$

Since the function f is a scalar variable, while we can confirm easily the rationality of this transformation by substituting Eq. (6) into Eq. (12), noting the equation

$$\mathbf{a}\bullet(\mathbf{\Omega a})=0, \tag{15}$$

for an arbitrary vector $\mathbf{a}$.

2.3. Evolution rule of the normal-sliding ratio

It can be assumed that the normal-sliding ratio increases with the sliding velocity, i.e.,

$$\overset{\bullet}{R}=U(R)\|\mathbf{r}^{\mathrm{p}}\| \quad \text{for } \mathbf{r}^{\mathrm{p}}\neq\mathbf{0}, \tag{16}$$

where U is a monotonically decreasing function of R fulfilling the following conditions (see Fig. 1).

$$\left.\begin{array}{ll} U=+\infty & \text{for } R=0,\\ U=0 & \text{for } R=1,\\ (U<0 & \text{for } R>1).\end{array}\right\} \tag{17}$$

2.4. Sliding velocity

The substitution of Eq. (16) into Eq. (14) gives rise to the *consistency condition* for the sliding-subloading surface:

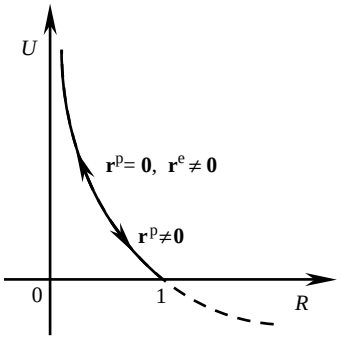

Fig. 1. Function U for the evolution rule of the normal-friction ratio R.

$$\frac{\partial f}{\partial\|\mathbf{f}_{\mathrm{n}}\|}\mathbf{n}\bullet\overset{\circ}{\mathbf{f}}_{\mathrm{n}}+\frac{\partial f}{\partial\|\mathbf{f}_{\mathrm{t}}\|}\mathbf{t}\bullet\overset{\circ}{\mathbf{f}}_{\mathrm{t}}=U\|\mathbf{r}^{\mathrm{p}}\|F+R\dot{F}. \tag{18}$$

Assume the following *sliding flow rule*,

$$\mathbf{r}^{\mathrm{p}}=\lambda\mathbf{p}\quad(\lambda>0,\ \ \|\mathbf{p}\|=1), \tag{19}$$

where λ is a positive proportionality factor and $\mathbf{p}$ is the unit vector. Substituting Eq. (19) into Eq. (18), the proportionality factor λ is derived as follows:

$$\lambda=\frac{\frac{\partial f}{\partial\|\mathbf{f}_{\mathrm{n}}\|}\mathbf{n}\bullet\overset{\circ}{\mathbf{f}}_{\mathrm{n}}+\frac{\partial f}{\partial\|\mathbf{f}_{\mathrm{t}}\|}\mathbf{t}\bullet\overset{\circ}{\mathbf{f}}_{\mathrm{t}}}{RF'h+UF}, \tag{20}$$

where h is a homogeneous degree-one function of H and $\mathbf{p}$, which is related to $\dot{H}$ as

$$h=\dot{H}/\lambda, \tag{21}$$

noting that $\dot{H}$ is a homogeneous function of degree-one in $\mathbf{r}^{\mathrm{p}}(=\lambda\mathbf{p})$, since it holds that $\dot{H}=0$ if $\mathbf{r}^{\mathrm{p}}=\mathbf{0}$ and the present model is concerned with the time-independent behavior and thus $\dot{H}$ has the dimension of minus one in time.

2.5. Traction rate-relative velocity relation

The expression of the relative velocity in terms of the traction rate is given from Eqs. (1), (4), (5), (19) and (20) as follows:

$$\begin{aligned}\mathbf{r}&=(\mathbf{r}_{\mathrm{n}}^{\mathrm{e}}+\mathbf{r}_{\mathrm{n}}^{\mathrm{p}})+(\mathbf{r}_{\mathrm{t}}^{\mathrm{e}}+\mathbf{r}_{\mathrm{t}}^{\mathrm{p}})=-\frac{1}{\alpha_{\mathrm{n}}}\overset{\circ}{\mathbf{f}}_{\mathrm{n}}+\lambda(\mathbf{p}\bullet\mathbf{n})\mathbf{n}-\frac{1}{\alpha_{\mathrm{t}}}\overset{\circ}{\mathbf{f}}_{\mathrm{t}}+\lambda(\mathbf{p}\bullet\mathbf{t})\mathbf{t}\\&=-\frac{1}{\alpha_{\mathrm{n}}}\overset{\circ}{\mathbf{f}}_{\mathrm{n}}+\frac{\frac{\partial f}{\partial\|\mathbf{f}_{\mathrm{n}}\|}\mathbf{n}\bullet\overset{\circ}{\mathbf{f}}_{\mathrm{n}}+\frac{\partial f}{\partial\|\mathbf{f}_{\mathrm{t}}\|}\mathbf{t}\bullet\overset{\circ}{\mathbf{f}}_{\mathrm{t}}}{RF'h+UF}(\mathbf{p}\bullet\mathbf{n})\mathbf{n}-\frac{1}{\alpha_{\mathrm{t}}}\overset{\circ}{\mathbf{f}}_{\mathrm{t}}+\frac{\frac{\partial f}{\partial\|\mathbf{f}_{\mathrm{n}}\|}\mathbf{n}\bullet\overset{\circ}{\mathbf{f}}_{\mathrm{n}}+\frac{\partial f}{\partial\|\mathbf{f}_{\mathrm{t}}\|}\mathbf{t}\bullet\overset{\circ}{\mathbf{f}}_{\mathrm{t}}}{RF'h+UF}(\mathbf{p}\bullet\mathbf{t})\mathbf{t}.\end{aligned} \tag{22}$$

The substitution of Eqs. (4), (5) and (19) into Eq. (18) leads to

$$-\alpha_{\mathrm{n}}\frac{\partial f}{\partial\|\mathbf{f}_{\mathrm{n}}\|}\mathbf{n}\bullet(\mathbf{r}_{\mathrm{n}}-\mathbf{r}_{\mathrm{n}}^{\mathrm{p}})-\alpha_{\mathrm{t}}\frac{\partial f}{\partial\|\mathbf{f}_{\mathrm{t}}\|}\mathbf{t}\bullet(\mathbf{r}_{\mathrm{t}}-\mathbf{r}_{\mathrm{t}}^{\mathrm{p}})=U\lambda F+RF'\lambda h,$$

which is further rewritten as

$$-\alpha_{\mathrm{n}}\frac{\partial f}{\partial\|\mathbf{f}_{\mathrm{n}}\|}\mathbf{n}\bullet\{\mathbf{n}\otimes\mathbf{n}\mathbf{r}-\lambda(\mathbf{p}\bullet\mathbf{n})\mathbf{n}\}-\alpha_{\mathrm{t}}\frac{\partial f}{\partial\|\mathbf{f}_{\mathrm{t}}\|}\mathbf{t}\bullet\{(\mathbf{I}-\mathbf{n}\otimes\mathbf{n})\mathbf{r}-\lambda(\mathbf{p}\bullet\mathbf{t})\mathbf{t}\}=U\lambda F+RF'\lambda h \tag{23}$$

by Eqs. (2), (4), and (19). The proportionality factor λ expressed in terms of the relative velocity, rewritten as Λ, is given by

$$\Lambda=\frac{-\left(\alpha_{\mathrm{n}}\frac{\partial f}{\partial\|\mathbf{f}_{\mathrm{n}}\|}\mathbf{n}+\alpha_{\mathrm{t}}\frac{\partial f}{\partial\|\mathbf{f}_{\mathrm{t}}\|}\mathbf{t}\right)\bullet\mathbf{r}}{RF'h+UF-\alpha_{\mathrm{n}}\frac{\partial f}{\partial\|\mathbf{f}_{\mathrm{n}}\|}(\mathbf{p}\bullet\mathbf{n})-\alpha_{\mathrm{t}}\frac{\partial f}{\partial\|\mathbf{f}_{\mathrm{t}}\|}(\mathbf{p}\bullet\mathbf{t})}. \tag{24}$$

The rate of traction is given from Eqs. (1)–(5), (19) and (24) as

$$\begin{aligned}\overset{\circ}{f}&=-\alpha_{\mathrm{n}}(\mathbf{r}_{\mathrm{n}}-\mathbf{r}_{\mathrm{n}}^{\mathrm{p}})-\alpha_{\mathrm{t}}(\mathbf{r}_{\mathrm{t}}-\mathbf{r}_{\mathrm{t}}^{\mathrm{p}})=-\alpha_{\mathrm{n}}\{(\mathbf{n}\otimes\mathbf{n})\mathbf{r}-\Lambda(\mathbf{p}\bullet\mathbf{n})\mathbf{n}\}-\alpha_{\mathrm{t}}\{(\mathbf{I}-\mathbf{n}\otimes\mathbf{n})\mathbf{r}-\Lambda(\mathbf{p}\bullet\mathbf{t})\mathbf{t}\}\\&=\mathbf{C}^{\mathrm{f}}\mathbf{r},\end{aligned} \tag{25}$$

where $\mathbf{C}^{\mathrm{f}}$ is the frictional stiffness modulus, i.e.,

$$\mathbf{C}^{\mathrm{f}} \equiv -\left[\alpha_{\mathrm{t}}\mathbf{I} + (\alpha_{\mathrm{n}} - \alpha_{\mathrm{t}})(\mathbf{n}\otimes\mathbf{n}) + \frac{\{\alpha_{\mathrm{n}}(\mathbf{p}\bullet\mathbf{n})\mathbf{n} + \alpha_{\mathrm{t}}(\mathbf{p}\bullet\mathbf{t})\mathbf{t}\}\otimes\left(\alpha_{\mathrm{n}}\frac{\partial f}{\partial\|\mathbf{f}_{\mathrm{n}}\|}\mathbf{n} + \alpha_{\mathrm{t}}\frac{\partial f}{\partial\|\mathbf{f}_{\mathrm{t}}\|}\mathbf{t}\right)}{RF'h + UF - \alpha_{\mathrm{n}}\frac{\partial f}{\partial\|\mathbf{f}_{\mathrm{n}}\|}(\mathbf{p}\bullet\mathbf{n}) - \alpha_{\mathrm{t}}\frac{\partial f}{\partial\|\mathbf{f}_{\mathrm{t}}\|}(\mathbf{p}\bullet\mathbf{t})}\right]. \tag{26}$$

For the case of $\mathbf{p} = -\mathbf{t}$, Eq. (26) becomes

$$\mathbf{C}^{\mathrm{f}} = -\left\{\alpha_{\mathrm{t}}\mathbf{I} + (\alpha_{\mathrm{n}} - \alpha_{\mathrm{t}})(\mathbf{n}\otimes\mathbf{n}) - \frac{\alpha_{\mathrm{t}}\mathbf{t}\otimes\left(\alpha_{\mathrm{n}}\frac{\partial f}{\partial\|\mathbf{f}_{\mathrm{n}}\|}\mathbf{n} + \alpha_{\mathrm{t}}\frac{\partial f}{\partial\|\mathbf{f}_{\mathrm{t}}\|}\mathbf{t}\right)}{RF'h + UF + \alpha_{\mathrm{t}}\frac{\partial f}{\partial\|\mathbf{f}_{\mathrm{t}}\|}}\right\}, \tag{27}$$

which further reduces for $F = \text{const}$ to

$$\mathbf{C}^{\mathrm{f}} = -\left\{\alpha_{\mathrm{t}}\mathbf{I} + (\alpha_{\mathrm{n}} - \alpha_{\mathrm{t}})(\mathbf{n}\otimes\mathbf{n}) - \frac{\alpha_{\mathrm{t}}\mathbf{t}\otimes\left(\alpha_{\mathrm{n}}\frac{\partial f}{\partial\|\mathbf{f}_{\mathrm{n}}\|}\mathbf{n} + \alpha_{\mathrm{t}}\frac{\partial f}{\partial\|\mathbf{f}_{\mathrm{t}}\|}\mathbf{t}\right)}{UF + \alpha_{\mathrm{t}}\frac{\partial f}{\partial\|\mathbf{f}_{\mathrm{t}}\|}}\right\}, \tag{28}$$

where $\mathbf{p} = -\mathbf{t}$ and/or $F = \text{const}$ would hold at a usual level of normal traction for which the gap between contact surfaces does not change.

The loading criterion for the sliding velocity is given as follows:

$$\left.\begin{array}{l}\mathbf{r}^{\mathrm{p}} \neq \mathbf{0} : \Lambda > 0,\\ \mathbf{r}^{\mathrm{p}} = \mathbf{0} : \Lambda \leqslant 0\end{array}\right\} \tag{29}$$

due to the requirement of positiveness for the proportionality factor Λ (Hashiguchi, 1994, 2000).

Eq. (22) for the relative velocity is obtained by substituting the sliding flow rule (19) into the consistency condition (18), which is obtained by incorporating the evolution rule (16) of the normal-sliding ratio R into the material-time derivative (12) of Eq. (11) for the sliding-subloading surface. Then, the sliding velocity progresses gradually as the traction approaches the normal-sliding surface, exhibiting a *smooth elastic–plastic transition*. Thus, it fulfills the *smoothness condition* defined to require that "the traction rate–relative velocity relation changes continuously for a continuous change of traction." This can be expressed mathematically as follows:

$$\lim_{\delta\mathbf{f}\to\mathbf{0}} \mathbf{C}^{\mathrm{f}}(\mathbf{f} + \delta\mathbf{f}, H, \mathbf{r}) = \mathbf{C}^{\mathrm{f}}(\mathbf{f}, H, \mathbf{r}), \tag{30}$$

where $\delta(\ )$ stands for an infinitesimal variation and the response of the traction rate to the relative velocity in the current state of traction and internal variables is designated by $\mathbf{C}^{\mathrm{f}}(\mathbf{f}, H, \mathbf{r})$. Eq. (30) is based on the smoothness condition for constitutive equations proposed by Hashiguchi (1993a,b, 1997, 2000). Therefore, the present model has the following notable advantages:

(1) It predicts a smooth response to a smooth monotonic frictional loading. In contrast, a non-smooth response is predicted by conventional friction models that violate the smoothness condition, which assumes the sliding surface enclosing a purely elastic domain.
(2) Only a decision regarding the sign of the quantity Λ is required in the loading criterion (29) of the present model, since the traction always lies on the sliding-subloading surface, which plays the role of the loading surface. In conventional friction models, however, a judgment whether or not the sliding condition is fulfilled is required in addition to the decision for the sign of Λ.
(3) In the numerical calculation, the traction is automatically drawn back to the normal-sliding surface even if it goes out from that surface since it is formulated such that $\dot{R} > 0$ for $R < 1$ (sub-sliding state: $f < F(H)$) and $\dot{R} < 0$ for $R > 1$ (over normal-sliding state: $f > F(H)$) in Eq. (16) with condition (17) as illustrated in Fig. 2. Thus, the present model allows a rough numerical calculation with large loading

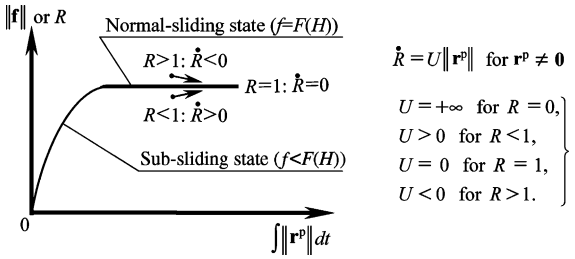

Fig. 2. Automatic controlling function of the present model to make a traction approach the normal-sliding surface in the plastic frictional loading process.

steps even in the explicit numerical calculation method. In conventional models, on the other hand, a special algorithm (cf. e.g. Euler method (Yamada et al., 1968), the radial return method (Krieg and Krieg, 1977), and the mean normal method (Pillinger et al., 1986)) has to be incorporated for pulling the traction back to the sliding surface so as not to go out from the surface in the explicit method.

3. Concrete constitutive equations

Formulated below are concrete constitutive equations for friction, in which concrete forms of material functions are proposed.

Soils having a frictional property exhibit a closed yield surface that depends on a pressure (cf. Roscoe and Burland, 1968; Schofield and Wroth, 1968). On the other hand, metals without a frictional property exhibit an open yield surface independent of pressure. However, as is observed in uniaxial compression or punch indentation phenomena, metals undergo a plastic deformation in a high level of normal traction, while the hardening of normal-sliding surface has to be introduced since the adhesion of asperities on the contact surface would grow in that level. Thus, the normal-sliding surface would in general form a closed surface in the traction vector space, although the open surfaces such as the cone of Coulomb and the parabolic surface have been widely adopted (e.g., Seguchi et al., 1974; Curnier, 1984; Wriggers et al., 1990).

We adopt the following quadric surface for the normal-sliding surface (Fig. 3):

$$f(\|\mathbf{f}_{\mathrm{n}}\|, \|\mathbf{f}_{\mathrm{t}}\|) = \frac{\|\mathbf{f}_{\mathrm{n}}\|}{1-\chi/2}, \tag{31}$$

where

$$\eta \equiv \frac{\|\mathbf{f}_{\mathrm{t}}\|}{\|\mathbf{f}_{\mathrm{n}}\|}, \quad \chi \equiv \frac{\eta}{M}. \tag{32}$$

M is a material constant depending on the frictional property. It holds for Eq. (31) that $\chi < 2$ and

$$\left.\begin{aligned} \frac{\partial f}{\partial \|\mathbf{f}_{\mathrm{n}}\|} &= -\frac{4(1-\chi)}{(2-\chi)^2}, \\ \frac{\partial f}{\partial \|\mathbf{f}_{\mathrm{t}}\|} &= \frac{2}{M(2-\chi)^2}, \\ \frac{\partial f}{\partial \|\mathbf{f}_{\mathrm{t}}\|} \Big/ \frac{\partial f}{\partial \|\mathbf{f}_{\mathrm{n}}\|} &= \frac{1}{2M(1-\chi)} \end{aligned}\right\} \tag{33}$$

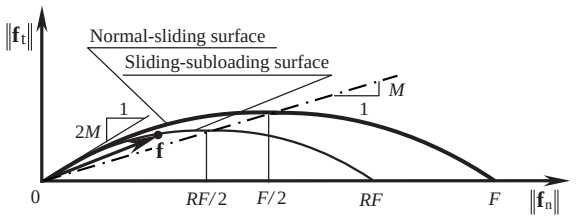

Fig. 3. Quadric normal-sliding and sliding-subloading surfaces of Eq. (31).

for which Eq. (28) becomes

$$\mathbf{C}^{\mathrm{f}} = -\left[\alpha_{\mathrm{t}}\mathbf{I} + (\alpha_{\mathrm{n}} - \alpha_{\mathrm{t}})(\mathbf{n}\otimes\mathbf{n}) - \frac{\alpha_{\mathrm{t}}\mathbf{t}\otimes\{2\alpha_{\mathrm{n}}M(1-\chi)\mathbf{n} + \alpha_{\mathrm{t}}\mathbf{t}\}}{MUF(2-\chi)^2/2 + \alpha_{\mathrm{t}}}\right]. \tag{34}$$

Furthermore, we assume the following tear-shaped surface for the normal-sliding surface (Fig. 4), which was first proposed for the yield surface of soils by Hashiguchi (1972, 1985):

$$f(\|\mathbf{f}_{\mathrm{n}}\|, \|\mathbf{f}_{\mathrm{t}}\|) = \|\mathbf{f}_{\mathrm{n}}\| \exp\left(\frac{\chi^2}{2}\right). \tag{35}$$

It holds for Eq. (35) that

$$\left.\begin{aligned} &\frac{\partial f}{\partial\|\mathbf{f}_{\mathrm{n}}\|} = (1-\chi^2)\exp\left(\frac{\chi^2}{2}\right),\\ &\frac{\partial f}{\partial\|\mathbf{f}_{\mathrm{t}}\|} = \frac{\chi}{M}\exp\left(\frac{\chi^2}{2}\right),\\ &\frac{\partial f}{\partial\|\mathbf{f}_{\mathrm{t}}\|}\Big/\frac{\partial f}{\partial\|\mathbf{f}_{\mathrm{n}}\|} = \frac{\chi}{M(1-\chi^2)} \end{aligned}\right\} \tag{36}$$

for which Eq. (28) becomes

$$\mathbf{C}^{\mathrm{f}} = -\left[\alpha_{\mathrm{t}}\mathbf{I} + (\alpha_{\mathrm{n}} - \alpha_{\mathrm{t}})(\mathbf{n}\otimes\mathbf{n}) - \frac{\alpha_{\mathrm{t}}\mathbf{t}\otimes\left\{\alpha_{\mathrm{n}}(1-\chi^2)\mathbf{n} + \alpha_{\mathrm{t}}\frac{\chi}{M}\mathbf{t}\right\}}{\frac{UF}{\exp(\chi^2/2)} + \alpha_{\mathrm{t}}\frac{\chi}{M}}\right]. \tag{37}$$

The hardening of the normal-sliding surface has to be introduced by which the traction would reach the critical state $\chi = 1$ as is observed in the soil behavior, whilst a further due consideration is required for the frictional behavior on a high normal-traction state.

The simplest function U for the rate of normal-sliding ratio R fulfilling Eq. (17), is given by

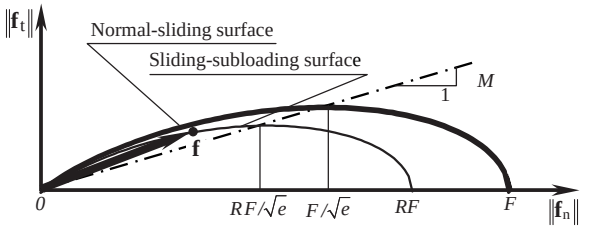

Fig. 4. Tear-shaped normal-sliding and sliding-subloading surfaces of Eq. (35).

$$U = -u \ln R, \tag{38}$$

where u is a material constant.

4. Basic response of the present model

Below, we examine the basic response of the present friction model to an input of relative tangential velocity under a constant normal traction.

In the coordinate system (n, t, s) of Fig. 5, let us select

$$\mathbf{n} = \begin{Bmatrix} 1 \\ 0 \\ 0 \end{Bmatrix}, \quad \mathbf{t} = \begin{Bmatrix} 0 \\ 1 \\ 0 \end{Bmatrix}, \quad \mathbf{f} = \begin{Bmatrix} f_{\mathrm{n}} \\ f_{\mathrm{t}} \\ 0 \end{Bmatrix}, \quad \mathbf{r} = \begin{Bmatrix} 0 \\ -r_{\mathrm{t}} \\ 0 \end{Bmatrix}, \tag{39}$$

$$f_{\mathrm{n}} \equiv \|\mathbf{f}_{\mathrm{n}}\| = \bar{r}F, \quad f_{\mathrm{t}} \equiv \|\mathbf{f}_{\mathrm{t}}\|, \quad \chi \equiv \frac{\|\mathbf{f}_{\mathrm{t}}\|/\|\mathbf{f}_{\mathrm{n}}\|}{M} = \frac{f_{\mathrm{t}}}{\bar{r}FM}, \quad r_{\mathrm{t}} \equiv \|\mathbf{r}_{\mathrm{t}}\|, \tag{40}$$

where $\bar{r}$ is a constant. The quadric surface (31) and the tear-shaped surface (31) and (35) are adopted for the normal-sliding surface. Let Eq. (38) be adopted for the function U.

For the quadric sliding surface (31), it holds that

$$R = \frac{\bar{r}}{1 - \chi/2}, \quad U = -u \ln\left(\frac{\bar{r}}{1 - \chi/2}\right), \tag{41}$$

$$\mathrm{d}f_{\mathrm{t}} = -\alpha_{\mathrm{t}}\left[1 - \frac{\alpha_{\mathrm{t}}}{-\frac{MuF}{2}\ln\left(\frac{2\bar{r}^2FM}{2\bar{r}FM - f_{\mathrm{t}}}\right)\left(2 - \frac{ft}{2\bar{r}FM}\right)^2 + \alpha_{\mathrm{t}}}\right]\mathrm{d}u_{\mathrm{t}}, \tag{42}$$

or

$$\mathrm{d}u_{\mathrm{t}} = -\frac{1}{\alpha_{\mathrm{t}}}\left[1 - \frac{\alpha_{\mathrm{t}}}{\frac{MuF}{2}\ln\left(\frac{2\bar{r}^2FM}{2\bar{r}FM - f_{\mathrm{t}}}\right)\left(2 - \frac{f_{\mathrm{t}}}{2\bar{r}FM}\right)^2}\right]\mathrm{d}f_{\mathrm{t}}, \tag{43}$$

where $\mathrm{d}u_{\mathrm{t}} = r_{\mathrm{t}}\,\mathrm{d}t$ (t: time) and $\mathrm{d}(\ ) = (\bullet)\,\mathrm{d}t$ denotes an increment. It holds that

$$f_{\mathrm{t}}^{n} = 2\bar{r}(1 - \bar{r})MF, \tag{44}$$

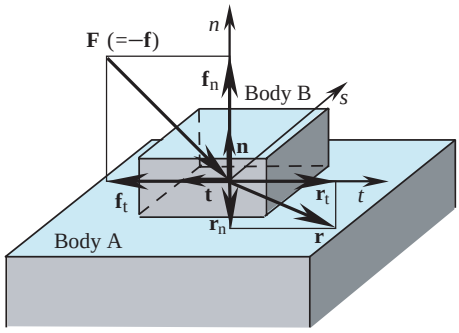

Fig. 5. Relative velocity **r** of body A with respect to body B and traction **f** acting body A in the coordinate system (n, t, s).

where f_{t}^{n} is the tangential traction on the normal-sliding surface for the normal traction $\bar{r}F$ in the present model.

For the tear-shaped sliding surface (35), it holds that

$$R = \bar{r}\exp(\chi^2/2), \quad U = -u\ln\{\bar{r}\exp(\chi^2/2)\}, \tag{45}$$

$$\mathrm{d}f_{\mathrm{t}} = -\alpha_{\mathrm{t}}\left[1 - \frac{\alpha_{\mathrm{t}} f_{\mathrm{t}} \exp\left\{\frac{1}{2}\left(\frac{f_{\mathrm{t}}}{\bar{r}FM}\right)^2\right\}}{-u\bar{r}(MF)^2 \ln\left\{\bar{r}\exp\left\{\frac{1}{2}\left(\frac{f_{\mathrm{t}}}{\bar{r}FM}\right)^2\right\}\right\} + \alpha_{\mathrm{t}} f_{\mathrm{t}} \exp\left\{\frac{1}{2}\left(\frac{f_{\mathrm{t}}}{\bar{r}FM}\right)^2\right\}}\right]\mathrm{d}u_{\mathrm{t}} \tag{46}$$

or

$$\mathrm{d}u_{\mathrm{t}} = -\frac{1}{\alpha_{\mathrm{t}}}\left[1 - \frac{\alpha_{\mathrm{t}} f_{\mathrm{t}} \exp\left\{\frac{1}{2}\left(\frac{f_{\mathrm{t}}}{\bar{r}FM}\right)^2\right\}}{u\bar{r}(MF)^2 \ln\left\{\bar{r}\exp\left\{\frac{1}{2}\left(\frac{f_{\mathrm{t}}}{\bar{r}FM}\right)^2\right\}\right\}}\right]\mathrm{d}f_{\mathrm{t}} \tag{47}$$

for which the tangential traction in the normal-sliding state is given by

$$f_{\mathrm{t}}^{n} = \bar{r}\sqrt{2\ln(1/\bar{r})}MF. \tag{48}$$

For the present calculation let the material parameters and the normal traction be selected as follows:

$$F = 100\,\mathrm{GPa}, \quad M = 0.3, \quad \alpha_t = 100\,\mathrm{GPa/mm}, \quad \bar{r} = 0.1.$$

The relationships of the dimensionless tangential traction $f_{\mathrm{t}}/f_{\mathrm{t}}^{n}$ versus the tangential relative displacement u_{t} due to Eqs. (42) and (46) are shown in Figs. 6 and 7, respectively. The smooth curves are predicted as have been observed in experiments by Rabinowicz (1951, 1965), Burwell and Rabinowicz (1953), Johnson (1955), Courtney-Pratt and Eisner (1957), Banerjee (1968), Johannes et al. (1973), and many others. The rate of approach of the traction to the normal-sliding surface can be controlled by the material constant u. The tangential traction–relative displacement relations in the classical friction model with rigid-plasticity and the conventional friction model with an abrupt elastic–plastic transition are also depicted in Figs. 6 and 7. Furthermore, Fig. 8 shows the measured and predicted (a) monotonic and (b) cyclic frictional

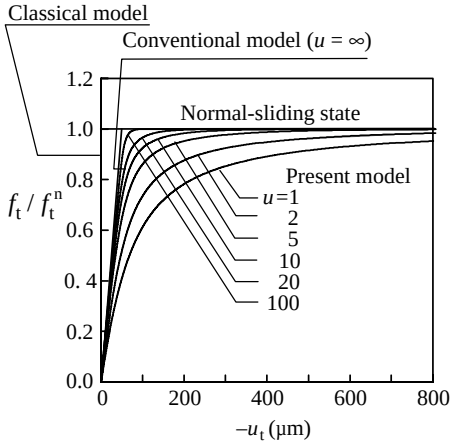

Fig. 6. Relationships of dimensionless tangential traction versus relative tangential displacement for the quadric sliding surface (31).

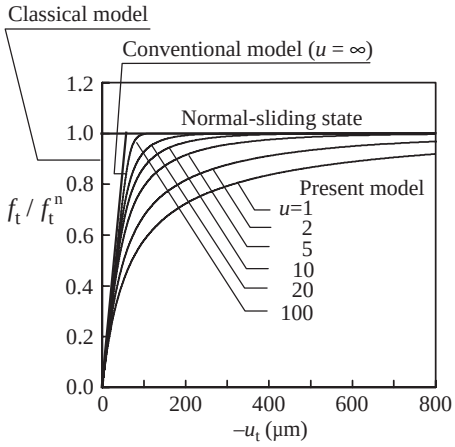

Fig. 7. Relationships of dimensionless tangential traction versus relative tangential displacement for the tear-shaped sliding surface (35).

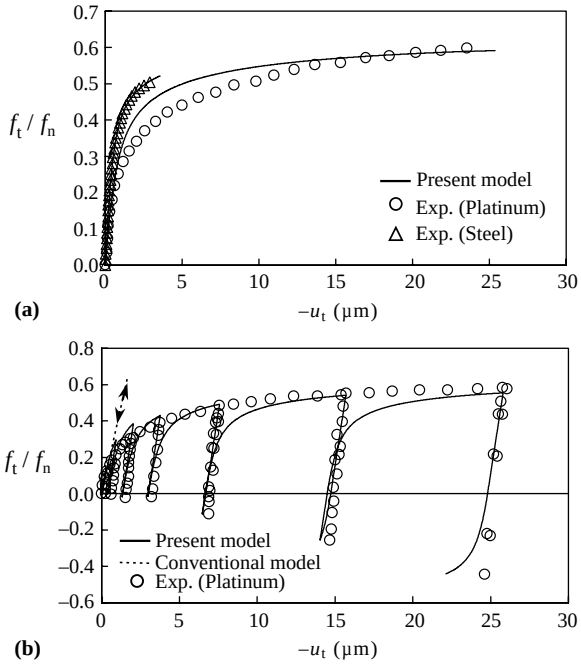

Fig. 8. The measured and predicted (a) monotonic and (b) cyclic frictional loading behavior for the polished metals (platinum-to-platinum for (a) and (b), and steel-to-steel for (a)) with clean surface (test data after Courtney-Pratt and Eisner, 1957).

loading behavior for the polished metals (platinum-to-platinum for (a) and (b) and steel-to-steel for (a)) with clean surface (test data after Courtney-Pratt and Eisner (1957)), while the tear-shaped sliding surface is adopted in the prediction. The material parameters for platinum-to-platinum are

$$F = 15\,\mathrm{GPa}, \quad M = 0.30, \quad \alpha_t = 1500\,\mathrm{GPa/mm}, \quad u = 40,$$

and steel-to-steel are

$$F = 12\,\mathrm{GPa}, \quad M = 0.30, \quad \alpha_{\mathrm{t}} = 1500\,\mathrm{GPa/mm}, \quad u = 150,$$

respectively. The predictions agree well with the test data.

5. Finite element discretization for boundary value problems

The finite element implementation incorporating the present friction model is described in this section. The main purpose of the present article is to exhibit the basic features and the advantages of the present constitutive model for friction. Then, the simple explicit numerical method of calculation is adopted traditionally, although the implicit method would be far more robust and efficient than the explicit method in the numerical calculations (cf. Wriggers, 2003).

5.1. Boundary conditions

Consider the deformation of a body, the boundary surface of which is denoted by Γ consisting of the prescribed traction rate boundary Γ_{t}, the prescribed displacement rate boundary Γ_v, and the contact boundary Γ_{c} as shown in Fig. 9. Since in general Γ_{c} changes during the deformation, the change has to be always judged by using the contact condition mentioned below throughout the calculation.

The gap (i.e., the minimum distance g_{n} from the boundary surface of the analyzing body to the surface of the external body) has to be zero and the normal component of the traction vector, f_{n}, applied to the body has to become positive when the bodies come into contact. Thus, the contact condition is given by

$$g_{\mathrm{n}} \geqslant 0, \quad f_{\mathrm{n}} \geqslant 0, \quad f_{\mathrm{n}} g_{\mathrm{n}} = 0, \tag{49}$$

where

$$f_{\mathrm{n}} = \mathbf{f} \bullet \mathbf{n} \tag{50}$$

$$g_{\mathrm{n}} \equiv (\mathbf{x}_{\Gamma}^{\mathrm{ext}} - \mathbf{x}_{\Gamma}) \bullet \mathbf{n}, \tag{51}$$

and $\mathbf{n}$ is the unit outward-normal vector on the boundary of the analyzing body. $\mathbf{x}_{\Gamma}$ is the position vector of the material point on the boundary surface of the analyzing body and $\mathbf{x}_{\Gamma}^{\mathrm{ext}}$ is the position vector of the material point on the surface of the external body.

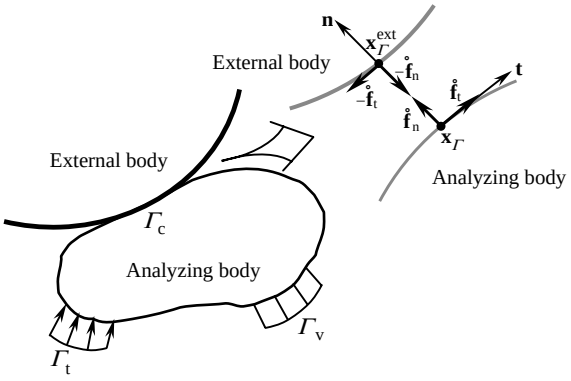

Fig. 9. Bodies in contact and boundary conditions.

The boundary conditions in the contact boundary of the analyzing body are given by

$$\left.\begin{array}{ll} \overset{\bullet}{\boldsymbol{\sigma}}\bullet\mathbf{n}=\mathbf{0} & \text{if } g_{\mathrm{n}}>0, \quad \text{on } \Gamma_{\mathrm{c}}, \\ \overset{\bullet}{\boldsymbol{\sigma}}\bullet\mathbf{n}=-\overset{\bullet}{\mathbf{f}} & \text{if } g_{\mathrm{n}}=0, \quad \text{on } \Gamma_{\mathrm{c}}, \end{array}\right\} \tag{52}$$

where $\boldsymbol{\sigma}$ is the Cauchy stress tensor.

The relative velocity $\mathbf{r}$ at the contact surface is given by

$$\mathbf{r}=\mathbf{v}_{\Gamma}^{\mathrm{ext}}-\mathbf{v}_{\Gamma} \tag{53}$$

where $\mathbf{v}_{\Gamma}$ and $\mathbf{v}_{\Gamma}^{\mathrm{ext}}$ are the velocities of the material points $\mathbf{x}_{\Gamma}$ and $\mathbf{x}_{\Gamma}^{\mathrm{ext}}$, respectively. Thus, it follows from Eqs. (25) and (53) that

$$\overset{\circ}{\mathbf{f}}=\mathbf{C}^{\mathrm{f}}(\mathbf{v}_{\Gamma}^{\mathrm{ext}}-\mathbf{v}_{\Gamma}). \tag{54}$$

5.2. Finite element discretization

The finite element discretization for the present friction model is described for the plane strain condition, assuming that the rigid-body rotation is negligible, and thus $\boldsymbol{\Omega}=\mathbf{0}$ and $\overset{\circ}{\mathbf{f}}=\overset{\bullet}{\mathbf{f}}$. The principle of the virtual work rate based on infinitesimal deformation theory is given by

$$\int_{V}\overset{\bullet}{\boldsymbol{\sigma}}\vdots\delta\mathbf{D}\,\mathrm{d}V=\int_{\Gamma_{\mathrm{t}}}\overset{\bullet}{\mathbf{t}}\bullet\delta\mathbf{v}\,\mathrm{d}S-\int_{\Gamma_{\mathrm{c}}}\overset{\bullet}{\mathbf{f}},\bullet\delta\mathbf{r}\,\mathrm{d}S, \tag{55}$$

where $\mathbf{D}$ and $\overset{\bullet}{\mathbf{t}}(\equiv\overset{\bullet}{\boldsymbol{\sigma}}\mathbf{N};\mathbf{N}$ stands for a normal vector on the prescribed traction rate boundary $\Gamma_{\mathrm{t}})$ are the strain rate (the symmetric part of the velocity gradient) and the traction rate. $\delta(\ )$ and $\vdots$ denote the virtual increment and the second-order scalar products, respectively.

The global stiffness equation given by the discretization of Eq. (55) is expressed as

$$[K]\{\mathrm{d}u\}=\{\mathrm{d}f\}-\{\mathrm{d}f^{\mathrm{c}}\}, \tag{56}$$

where $[K]$ is the stiffness matrix of the analyzing body, and $\{\mathrm{d}u\}$, $\{\mathrm{d}f\}$, and $\{\mathrm{d}f^{\mathrm{c}}\}$ are the nodal displacement, the nodal force, and the nodal contact force increment vectors, respectively. These terms in Eq. (56) are given as follows:

$$[K]=\Sigma_{e}V_{e}\mathbf{B}_{e}^{\mathrm{T}}\mathbf{C}_{e}^{\mathrm{m}}\mathbf{B}_{e}, \tag{57}$$

$$\{\mathrm{d}u\}=\Sigma_{\mathrm{n}}\mathbf{v}_{\mathrm{n}}\mathrm{d}t, \tag{58}$$

$$\{\mathrm{d}f\}=\Sigma_{e}S_{e}^{\mathrm{t}}\mathbf{N}_{e}^{\mathrm{T}}\overset{\bullet}{\mathbf{t}}_{e}\,\mathrm{d}t, \tag{59}$$

where $\mathbf{C}^{\mathrm{m}}$ is the stiffness modulus of analyzing body. Σ_{e} and Σ_{n} are the sums over all the elements and the nodal points, respectively.

Substituting Eq. (54) into the last term of Eq. (55) leads to

$$\{\mathrm{d}f^{\mathrm{c}}\}=\Sigma_{e}S_{e}^{\mathrm{c}}\mathbf{T}_{\mathrm{n}}^{\mathrm{T}}\mathbf{N}_{e}^{\mathrm{T}}\overset{\bullet}{\mathbf{f}}_{e}\,\mathrm{d}t=\Sigma_{e}S_{e}^{\mathrm{c}}\mathbf{T}_{\mathrm{n}}^{\mathrm{T}}\mathbf{N}_{e}^{\mathrm{T}}\mathbf{C}_{e}^{\mathrm{f}}\mathbf{N}_{e}\mathbf{T}_{\mathrm{n}}(\mathbf{v}_{\Gamma n}^{\mathrm{ext}}-\mathbf{v}_{\Gamma n})\,\mathrm{d}t=[K^{\mathrm{f}}]\{\mathrm{d}u^{\mathrm{ext}}\}-[K^{\mathrm{f}}]\{\mathrm{d}u\}, \tag{60}$$

where $\mathbf{B}_{e}$, $\mathbf{N}_{e}$, and $\mathbf{T}_{\mathrm{n}}$ are the strain increment–nodal displacement increment matrix, the shape function, and the transformation matrix between the local coordinate system (t,n) and the total coordinate system (x,y), $(\ )^{\mathrm{T}}$ denoting the transpose. V_{e} is the volume of the element, and S_{e}^{t} and S_{e}^{c} are the areas of the surfaces on the prescribed traction rate boundary and the contact boundary, respectively, in the element.

Substituting Eq. (60) into Eq. (56), the global stiffness equation is rewritten as

$$\left[[K]-[K^{\mathrm{f}}]\right]\{\mathrm{d}u\}=\{\mathrm{d}f\}-[K^{\mathrm{f}}]\{\mathrm{d}u^{\mathrm{ext}}\}. \tag{61}$$

It is observed in Eq. (61) that friction behavior is implemented into the finite element analysis as pseudo-elastoplastic deformation behavior.

6. Finite element analyses of frictional contact problems

In this section, we consider several typical frictional contact boundary value problems, specifically the compression of a rectangular block, the indentation of a cylindrical rigid roller into an elastic body, and the cyclic friction problem, in order to examine the validity of the present finite element program. The analyzing body is assumed to be of Hookean elastic material but the external body is rigid. In the calculation, the tear-shaped surface (35) for the normal-sliding surface and the frictional stiffness modulus (28) of $\mathbf{p}=-\mathbf{t}$ and $F=$ const. are adopted. The frictional stiffness modulus (28) leads to the unsymmetrical stiffness matrix since the non-associated flow rule with $\mathbf{p}=-\mathbf{t}$ is adopted for the sliding flow rule (19) and then it is solved by the ordinary Gauss elimination method with the band matrix optimization. Besides, the calculation is converged only by one incremental step without an iteration since the external and analyzing bodies are assumed to be the rigid and the elastic bodies, and optimum incremental step is adopted. That is, the calculation is attained by the incremental step more than 200 for 1% compression of the rectangular block and 1% indentation of the radius of the cylindrical rigid role, while the maximum tangential relative displacement increment is kept less than 1.0 μm.

Material parameters of the elastic body and the subloading-friction model are shown in Table 1, where E and v are the Young's modulus and Poisson's ratio, respectively. The friction coefficient $f_{\mathrm{n}}/f_{\mathrm{t}}$ for the normal-sliding surface is roughly evaluated to be 0.1–0.2 although the coefficient changes slightly with the normal traction for its usual range in the present model as illustrated in Figs. 3 and 4.

6.1. Compression of a rectangular block

The finite element mesh and boundary conditions for the compression of a rectangular block are shown in Fig. 10, while the analysis is formulated for 1/4 area due to the symmetry of the specimen.

The relationships between the tangential traction f_{t} and the relative tangential displacement u_{t} of the inside element (No. 10) and the outermost element (No. 20) on the contact surface at 10% compression are shown in Fig. 11(a) and (b). Similarly, the relationships between the normal-sliding ratio R and the relative tangential displacement u_{t} are shown in Fig. 11(c) and (d). Although the sliding displacement occurs suddenly when the traction fulfills the normal-sliding state for $u\to\infty$ leading to the conventional model, the smooth relationship between the tangential traction and the relative tangential displacement is described by the present program. Moreover, it is confirmed that the relative displacement increment by the increase in the traction is controlled by the material constant u.

Table 1
Material parameters

(a) Elastic body			
E	4 GPa	v	0.3
(b) Subloading-friction model			
F	100 GPa	M	0.05
$\alpha_{\mathrm{n}},\alpha_{\mathrm{t}}$	1000 GPa/mm	u	Four levels: 1, 10, 100 and ∞ (1000)

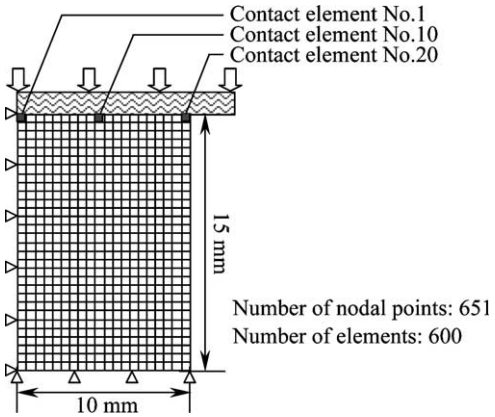

Fig. 10. Finite element mesh and boundary condition for the compression problem of rectangular block.

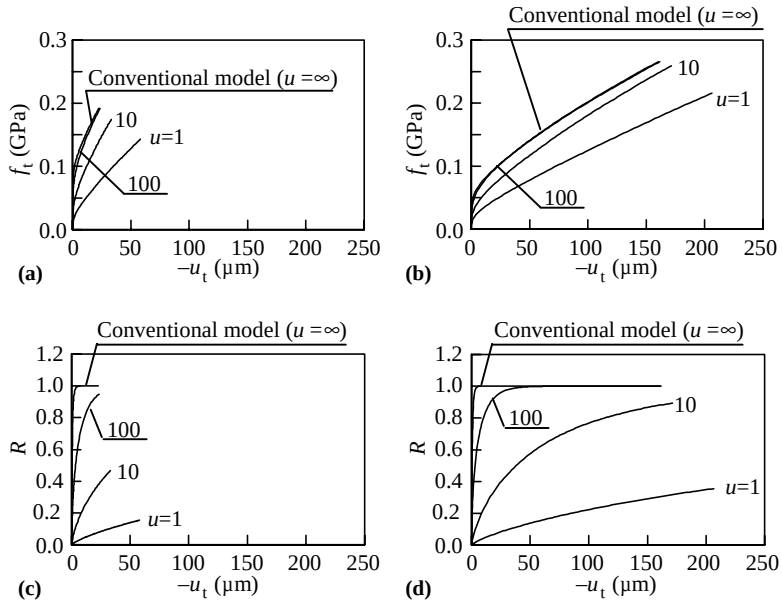

Fig. 11. Relationships between the tangential traction and the normal-sliding ratio to the relative tangential displacement inside and outside on the contact surface. (a) Contact element no. 10. (b) Contact element no. 20. (c) Contact element no. 10. (d) Contact element no. 20.

The distributions of normal traction f_n and tangential traction f_t on the contact surface at 10% compression are shown in Fig. 12(a) and (b), where the abscissa axes denote the contact element number. The distribution of the tangential traction becomes gentler for a smaller value of the material constant u for the evolution of the normal-yield ratio, but that of the normal traction is not affected by u.

6.2. Indentation problem of a cylindrical rigid roller

The finite element mesh and the boundary conditions for the indentation of a cylindrical rigid roller into an elastic body are shown in Fig. 13, while the analysis is formulated for 1/2 area for the symmetry of the

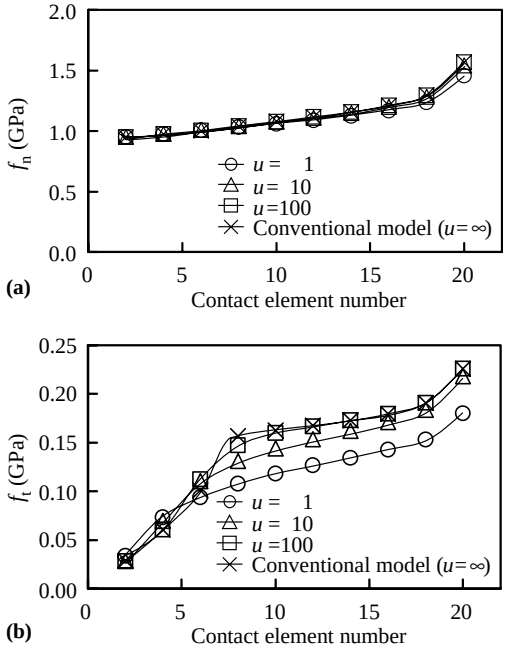

Fig. 12. Distribution of the contact traction on the contact surface (10% compression). (a) Normal traction. (b) Tangential tractial.

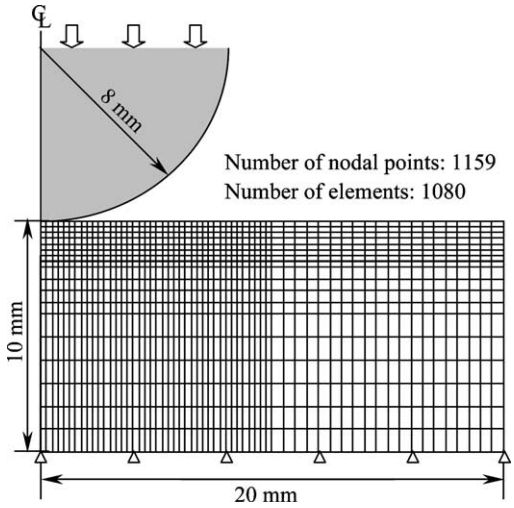

Fig. 13. Finite element mesh and boundary conditions for the problem of a rigid roller indenting an elastic body.

specimen. The lower end of the elastic specimen is fixed, and the cylindrical rigid roller is pushed vertically into the elastic body until the indentation reaches 20% of the roller radius.

The normal-traction distribution calculated by the finite element analysis for $u = 10$ is compared with the Hertz solution in Fig. 14 for 20% indentation of the roller radius. The axes of the ordinate and the abscissa

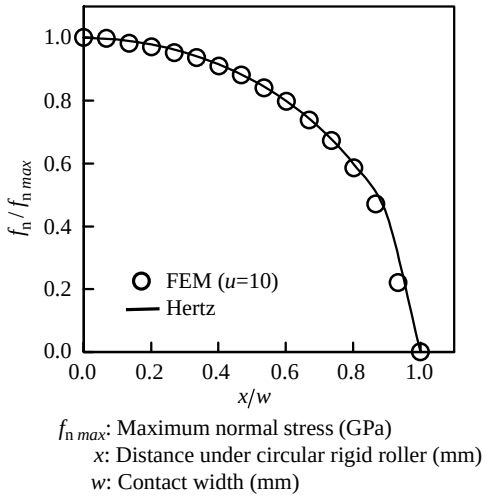

Fig. 14. Normal-traction distribution ($u = 10$) compared to the Hertz solution.

denote the dimensionless values of the normal traction and of the horizontal distance from the center of rigid roller, respectively, which are divided by each maximum value. The result by the finite element analysis is that of 20% indentation with $u = 10$. Note that the normal traction is largest just under the rigid roller, and it decreases smoothly towards the outer element; the distribution profile of the normal traction corresponds extremely well to the Hertz solution (Fig. 14).

The distributions of normal traction f_n, tangential traction f_t, and relative tangential displacement u_t for several levels of u at 20% indentation are shown in Fig. 15(a–c), where the abscissa axes denote the horizontal distance from the center of the rigid roller. The distribution profile of normal traction is not affected by the value of u and is predicted almost identical for all values of u. On the other hand, the distribution profile of tangential traction is influenced by the variation of u such that it becomes smaller for smaller values of u. Furthermore, the tangential displacement is larger for smaller values of u.

6.3. Cyclic friction problem

The finite element mesh and the boundary conditions for the cyclic friction problem are shown in Fig. 16, where the upper end of the specimen is the contact boundary but the lower end is fixed. Tangential tractions of constant amplitude are applied repeatedly under constant normal traction (5 GPa) on the contact boundary. In addition, the amplitude of the tangential traction is set to 3 levels: 10%, 50%, and 80% of tangential traction in the normal-sliding state for the set value of normal traction.

Relationships between the tangential traction f_t and the relative tangential displacement u_t for 3 levels of u are shown in Fig. 17, where the set value of the tangential traction is 80% of the above-mentioned tangential traction in the normal-sliding state. In the conventional friction model ($u \to \infty$), only the elastic relative tangential displacement is predicted for cyclic loading, and the accumulation of relative tangential displacement is not predicted at all. On the other hand, a realistic accumulation of the relative tangential displacement can be predicted in the present model since the sliding velocity is induced by the change of tangential traction inside the normal-sliding surface. Moreover, it is revealed that the amount of accumulation of the relative tangential displacement increases with decreasing values of u.

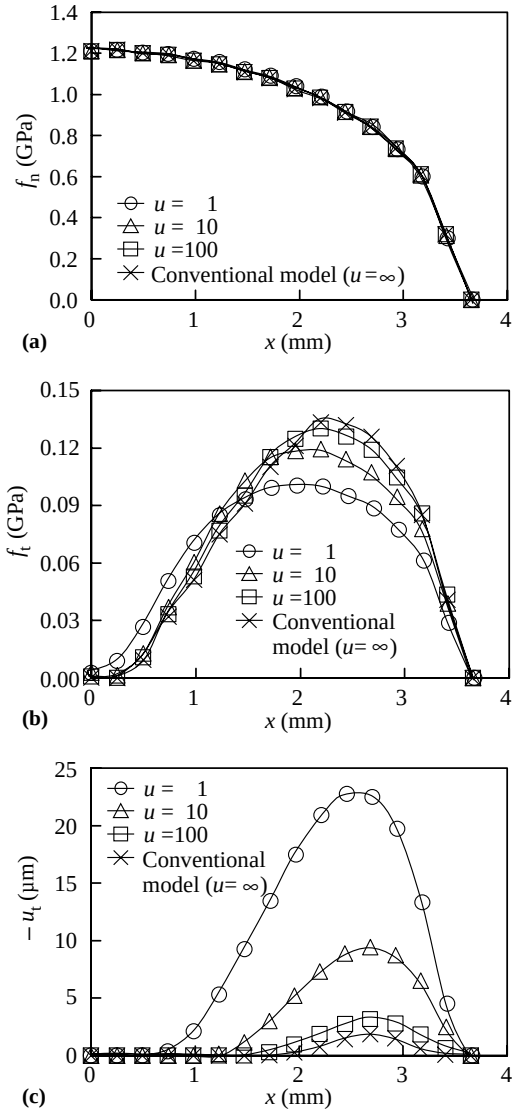

Fig. 15. Contact traction and relative tangential displacement distributions at 20% indentation. (a) Normal traction. (b) Tangential traction. (c) Relative tangential displacement.

Relationships between the tangential traction and the relative tangential displacement for various constant amplitudes of tangential traction with $u = 10$ are shown in Fig. 18. For all levels of the tangential traction, the accumulation of the relative tangential displacement is not predicted at all by the conventional friction model. The present finite element program, however, predicts the accumulation of the relative tangential displacement for any amplitude of tangential traction below the normal-sliding surface, and the amount of the accumulation depends on the magnitude of the tangential traction.

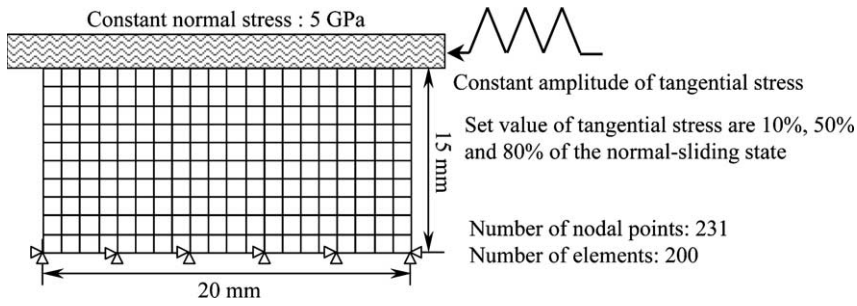

Fig. 16. Finite element mesh and boundary conditions for the cyclic friction problem.

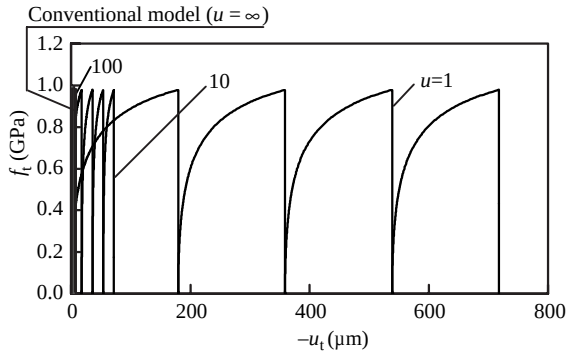

Fig. 17. Relationships between tangential traction and relative tangential displacement for various levels of u (amplitude: 80% of the maximum tangential stress).

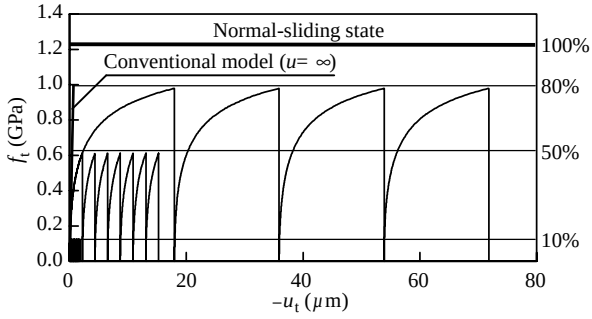

Fig. 18. Relationships between tangential traction and relative tangential displacement for various constant amplitudes of tangential traction for $u = 10$.

7. Concluding remarks

A constitutive model for the description of friction phenomena is formulated by incorporating the subloading surface concept (Hashiguchi, 1978, 1980, 1989). The following fundamental improvements are attained by the present model.

(1) The normal traction and the tangential traction are linearly related by the two material constants, i.e., the frictional angle ϕ and the adhesion c in the Coulomb sliding condition. On the other hand, they are related nonlinearly such that the slope of the normal traction–tangential traction curve decreases as the normal traction increases in the present model without an increase in number of material constants, i.e., two of M and F.
(2) In conventional friction models, the sliding displacement (plastic relative displacement) occurs suddenly when the traction fulfills the sliding condition. In contrast, in the present model, the sliding displacement progresses gradually as the tangential traction increases, exhibiting the smooth elastic–plastic transition, and thus the smooth relationship of the tangential traction versus the relative tangential displacement is described.
(3) Accumulation of the sliding displacement during cyclic loading of tangential traction below the sliding condition cannot be predicted by conventional models. On the other hand, it can be predicted in the present unconventional model, since the sliding displacement is induced by the rate of traction inside the normal-sliding surface. For instance, the loosening of a screw subjected to cyclic loading can be predicted by the present model. Moreover, it is widely known that the drawbar-pull of off-the-road vehicles increases gradually with the slippage induced by the relative displacement between wheels and soils (cf. Nohse et al., 1991; Hashiguchi et al., 1994; Shikanai et al., 2000). This phenomenon cannot be described by classical or conventional friction models since the tangential traction for the sliding condition is attained for null or infinitesimal tangential relative displacement and thus the maximum drawbar-pull is predicted even for null or infinitesimal slippage. In order to predict the phenomenon it is required to utilize unconventional friction model such as the present model.
(4) In a numerical calculation in conventional models, a special algorithm has to be incorporated for pulling the traction back to the sliding surface so as not to go out from the surface. In the present model, such an algorithm is not necessary since the traction is automatically drawn back to the normal-sliding surface even if it goes out from the surface.
(5) Conventional models require a loading criterion, i.e., a judgment of whether or not traction fulfills the sliding condition. The present model, however, does not require a loading criterion since the traction exists always on the sliding-subloading surface playing the role of the loading surface.
(6) It is possible to formulate the inverse relation, i.e., an expression of the relative velocity in terms of the traction rate.

The above-mentioned benefits (2)–(5) are obtained by introducing only one material parameter u in Eq. (38) for the evolution rule of the normal-sliding ratio R.

The present model is of a quite simple form involving only five material parameters, α_n, α_t, F, M and u, yet it enables us to describe realistically friction phenomena including cyclic frictional loading behavior. The evolution of the normal-sliding surface, however, is not taken into account in the concrete formulation. Thus, the differences between static and dynamic frictions cannot be predicted in the present concrete formulation, while dynamic friction has to be formulated as a rate-dependent behavior. More consideration of a concrete formulation for the evolution of the normal-sliding surface to predict the dynamic friction behavior would be required.

References

Asaoka, A., Nakano, M., Noda, T., 2000. Superloading yield surface concept for highly structured soil behaviour. Soils Found. 40 (2), 99–110.

Banerjee, A.E., 1968. Influence of kinetic friction on the critical velocity of stick-slip motion. Wear 12, 107–116.

Burwell, J.T., Rabinowicz, E., 1953. The nature of the static and kinetic coefficients of friction. J. Appl. Phys. 24, 136–139.

Cheng, J.-H., Kikuchi, N., 1985. An incremental constitutive relation of uniaxial contact friction for large deformation analysis. J. Appl. Mech. (ASME) 52, 639–648.

Courtney-Pratt, J.S., Eisner, E., 1957. The effect of a tangential force on the contact metallic bodies. Proc. Roy. Soc. London, Ser. A 238, 529–550.

Curnier, A., 1984. A theory of friction. Int. J. Solids Struct. 20, 637–647.

Drucker, D.C., 1988. Conventional and unconventional plastic response and representation. Appl. Mech. Rev. (ASME) 41, 151–167.

Fredriksson, B., 1976. Finite element solution of surface nonlinearities in structural mechanics with special emphasis to contact and fracture mechanics problems. Comput. Struct. 6, 281–290.

Hashiguchi, K., 1972. On the yielding of frictional plastic body—hardening rule. In: Proc. 27th Annual Meeting, JSCE, pp. 105–108.

Hashiguchi, K., 1978. Plastic constitutive equations of granular materials. In: Proc. US–Japan Seminar Continuum Mech. Stast. Appr. Mech. Granular Materials, Sendai, pp. 321–329.

Hashiguchi, K., 1980. Constitutive equations of elastoplastic materials with elastic–plastic transition. J. Appl. Mech. (ASME) 47, 266–272.

Hashiguchi, K., 1985. Macrometric approaches—static-intrinsically time-independent, Constitutive Laws of Soils (Proc. Discussion Session 1A of 11th ICSMFE), San Francisco, pp. 25–56.

Hashiguchi, K., 1989. Subloading surface model in unconventional plasticity. Int. J. Solids Struct. 25, 917–945.

Hashiguchi, K., 1993a. Fundamental requirements and formulation of elastoplastic constitutive equations with tangential plasticity. Int. J. Plasticity 9, 525–549.

Hashiguchi, K., 1993b. Mechanical requirements and structures of cyclic plasticity models. Int. J. Plasticity 9, 721–748.

Hashiguchi, K., 1994. On the loading criterion. Int. J. Plasticity 10, 871–878.

Hashiguchi, K., 1997. The extended flow rule in plasticity. Int. J. Plasticity 13, 37–58.

Hashiguchi, K., 2000. Fundamentals in constitutive equation: continuity and smoothness conditions and loading criterion. Soils Found. 40 (3), 155–161.

Hashiguchi, K., Chen, Z.-P., 1998. Elastoplastic constitutive equations of soils with the subloading surface and the rotational hardening. Int. J. Numer. Anal. Meth. Geomech. 22, 197–227.

Hashiguchi, K., Tsutsumi, S., 2003. Shear band formation analysis in soils by the subloading surface model with tangential stress rate effect. Int. J. Plasticity 19, 1651–1677.

Hashiguchi, K., Yoshimaru, T., 1995. A generalized formulation of the concept of nonhardening region. Int. J. Plasticity 11, 347–365.

Hashiguchi, K., Nohse, Y., Ueno, M., Sumiyoshi, K., Uchiyama, K., Yoshimaru, T., 1994. Traveling performance of a wheel on a finite thickness ground. J. Terramech. 31, 257–263.

Hashiguchi, K., Protasov, A.Y., Okayasu, T., 2001. Post-localization analysis by the subloading surface model with tangential stress rate effect. Mater. Sci. Res. Int. 7, 265–272.

Hashiguchi, K., Saitoh, K., Okayasu, T., Tsutsumi, S., 2002. Evaluation of typical conventional and unconventional plasticity models for prediction of softening behavior of soils. Geotechnique 52, 561–573.

Johannes, M.A., Green, M.A., Brockley, C.A., 1973. The role of the rate of application of the tangential force in determining the static friction coefficient. Wear 24, 381–385.

Johnson, K.L., 1955. Surface interaction between elastically loaded bodies under tangential forces. Proc. Roy. Soc. London, Ser. A 230, 531–548.

Krieg, R.D., Krieg, D.B., 1977. Accuracies of numerical solution methods for the elastic-perfectly plastic models. J. Pressure Vessel Tech. (ASME) 99, 510–515.

Michalowski, R., Mroz, Z., 1978. Associated and non-associated sliding rules in contact friction problems. Arch. Mech. 30, 259–276.

Nohse, Y., Hashiguchi, K., Shikanai, T., Ueno, M., Izumi, H., Koyama, F., 1991. A measurement of basic mechanical quantities of off-the-road traveling performance. J. Terramech. 28, 359–370.

Oden, J.T., Pires, E.B., 1983. Nonlocal and nonlinear friction laws and variational principles for contact problems in elasticity. Appl. Mech. (ASME) 50, 67–76.

Peric, D., Owen, R.J., 1992. Computational model for 3-D contact problems with friction based on the penalty method. Int. J. Numer. Methods Eng. 35, 1289–1309.

Pillinger, I., Hartley, P., Sturgess, C.E.N., Rowe, G.W., 1986. Use of a mean-normal large-strain elastic–plastic finite element solutions. Int. J. Mech. Sci. 28, 23–29.

Rabinowicz, E., 1951. The nature of the static and kinetic coefficients of friction. J. Appl. Phys. 22, 1373–1379.

Rabinowicz, E., 1965. Friction and Wear of Materials. John Wiley & Sons, New York.

Roscoe, K.H., Burland, J.B., 1968. On the generalized stress–strain behavior of 'wet' clay. In: Heyman, J., Leckie, F.A. (Eds.), Engineering Plasticity. Cambridge University Press, Cambridge, pp. 535–608.

Schofield, A.N., Wroth, C.P., 1968. Critical State Soil Mechanics. McGraw-Hill, London.

Seguchi, Y., Shindo, A., Tomita, Y., and Sunohara, M., 1974. Sliding rule of friction in plastic forming of metal. Computational Methods in Nonlinear Mechanics, University of Texas at Austin, pp. 683–692.

Shikanai, T., Hashiguchi, K., Nohse, Y., Ueno, M., Okayasu, T., 2000. Precise measurement of soil deformation and fluctuation in drawbar pull for steel and rubber-coated rigid wheels. J. Terramech. 37, 21–39.

Topolnicki, M., 1990. An elasto-plastic subloading surface model for clay with isotropic and kinematics mixed hardening parameters. Soils Found. 30 (2), 103–113.

Wriggers, P., 2003. Computational Contact Mechanics. J. Wiley, Chichester.

Wriggers, P., Vu Van, T., Stein, E., 1990. Finite element formulation of large deformation impact-contact problems with friction. Comput. Struct. 37, 319–331.

Yamada, Y., Yoshimura, N., Sakurai, T., 1968. Plastic stress–strain matrix and its application for the solution of elastic–plastic problems by finite element method. Int. J. Mech. Sci. 10, 343–354.